Extensibility of the Extended Tail Domain of Processive and Nonprocessive Myosin V Molecules

Attila Nagy,[†] Grzegorz Piszczek,[‡] and James R. Sellers[†*]
[†]Laboratory of Molecular Physiology and [‡]Biophysics Facility, National Heart, Lung and Blood Institute, National Institutes of Health, Bethesda, Maryland

ABSTRACT Myosin V is a single-molecule motor that moves organelles along actin. When myosin V pulls loads inside the cell in a highly viscous environment, the force on the motor is unlikely to be constant. We propose that the tether between the single-molecule motor and the cargo (i.e., the extended tail domain of the molecule) must be able to absorb the sudden mechanical motions of the motor and allow smooth relaxation of the motion of the cargo to a new position. To test this hypothesis, we compared the elastic properties of the extended tail domains of processive (mouse myosin Va) and nonprocessive (*Drosophila* myosin V) molecular motors. The extended tail domain of these myosins consists of mechanically strong coiled-coil regions interspersed with flexible loops. In this work we explored the mechanical properties of coiled-coil regions using atomic force microscopy. We found that the processive and nonprocessive coiled-coil fragments display different unfolding patterns. The unfolding of coiled-coil structures occurs much later during the atomic force microscopy stretch cycle for processive myosin Va than for nonprocessive *Drosophila* myosin V, suggesting that this elastic tether between the cargo and motor may play an important role in sustaining the processive motions of this single-molecule motor.

INTRODUCTION

Myosin Va is a double-headed, processive molecular motor that moves along actin filaments and transports a variety of cargos (1–4). In vivo, myosin Va moves melanosomes, synaptic vesicles, and other vesicular organelles. These cargos range in size from 50 nm to >1 μm in diameter (5,6).

Myosin Va shares common features with other members of the myosin superfamily (Fig. 1). The heavy chain of the molecule contains the motor domain, which is responsible for actin binding and ATP hydrolysis. The motor domain is followed by a 24 nm long neck region. The neck of the molecule consists of an α-helix containing six IQ motifs (consensus sequence IQxxxRGxxxR, where x denotes any amino acid), each of which binds a calmodulin (CaM) molecule, which stabilizes the helix (7). The elongated and rigid neck enables myosin Va molecules to take 36 nm steps (8,9), and also plays a crucial role in regulation of the motor (10–13). The extended tail domain is responsible for the dimerization of the molecule, and acts as a tether between the motor and the cargo. The C-terminal end of the molecule encodes the globular tail domain, which plays a role in two processes: it binds the cargo via cargo-specific receptors, and it interacts with the motor domain on the N-terminus, which folds the motor into a stable, inhibited conformation (13–16).

Myosin Va is a high duty ratio motor (8,17) that spends a large portion (>50%) of its enzymatic cycle strongly attached to the actin filament. The combination of its high duty ratio and the dimeric nature of the molecule, and its ability to take 36 nm steps (which corresponds to the length of the half-pitch of an actin filament) makes this motor a highly processive, optimized vesicle transporter (18).

Myosin Va moves along the actin filament in a hand-over-hand fashion (for review, see Sellers and Veigel (19)). At physiological concentrations of ATP and low external loads, the processive stepping of the molecule is limited by the ADP release rate from the trailing head (14,20). Numerous in vitro biochemical and biophysical studies have demonstrated that the kinetics of myosin Va is regulated by the load (21–23). In vivo, when a processive motor moves its cargo along actin filaments inside the crowded cellular environment, this load is unlikely to be constant. The viscosity of the cytosol is in the range of 3×10^{-3}–10^{3} Pa · s (24). A vesicle moved by myosin V through this viscous medium would generate a significant drag force opposite to the direction of the motion of the motor-cargo complex. As revealed by previous optical-trap and total internal reflection fluorescence microscopy in vitro experiments, the plot of distance traveled against time for myosin Va shows a characteristic staircase pattern, suggesting that the stepping motion of the motor occurs rapidly compared to the sampling rate of the assays, and that the motor dwells in an attached state in between steps (8,14). If the connection between the motor and the cargo is infinitely rigid, the vesicle should move in the same manner. In this case, the motor must exert a force large enough and over a sufficiently long time to make the vesicle follow its motion without any delay. If these conditions are met, moving a vesicle a distance as small as 0.1 μm at the speed of a myosin V (~1 μm/s) inside of the cell would require a sustained force of 100 pN, whereas the stall force of myosin Va molecule is ~2–3 pN (20,23,25). In the case of processive single-molecule vesicle transporters, a more flexible connection between the cargo and motor would be

Submitted May 12, 2009, and accepted for publication September 17, 2009.

*Correspondence: sellersj@nhlbi.nih.gov

Editor: E. Michael Ostap.

0006-3495/09/12/3123/9 $2.00

doi: 10.1016/j.bpj.2009.09.033

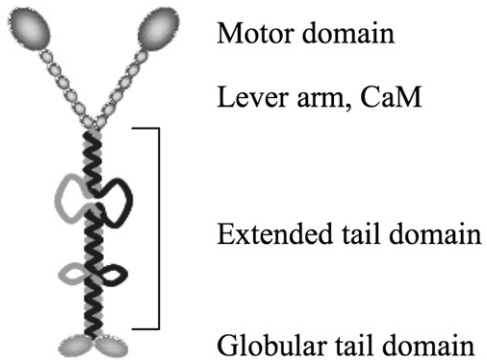

FIGURE 1 Domain structure of myosin Va.

desirable because a soft, spring-like element connecting the transported vesicle to myosin V could absorb the sudden impact of a rapid forward motion, and could also reduce the instantaneous backward pull on the motor.

In this study, we characterized the elastic properties of the extended tail domain of processive mouse (*Mm*) myosin Va using atomic force microscopy (AFM). To compare the elastic behavior of the extended tail domain from a processive and a nonprocessive myosin V molecule, we also characterized the homologous segment from the *Drosophila melanogaster* (*Dm*) myosin V molecule, a motor that has a lower duty ratio and likely functions in an ensemble (26).

While pulling a cargo, processive and nonprocessive myosin molecules must fulfill different requirements. Single-molecule motors must be able to move the cargo on a one-on-one basis; however, nonprocessive ensemble motors move the load with a combined effort, and thus the load on individual motors is shared and much less than in the case of processive single-molecule motors. Single-molecule motors such as *Mm* myosin Va need an elastic tether to work at a reasonable (lower than stall) force. In the case of nonprocessive ensemble motors such as *Dm* myosin V, the elastic connection enables molecules to step in asynchrony. To maximize the efficiency of the system, the tethers must have very specific elastic characteristics. The aim of our study was to compare the elastic properties of the tethers of a processive single-molecule motor and a nonprocessive ensemble motor.

MATERIALS AND METHODS

Single-molecule force spectroscopy

The segments were held specifically at their N-termini via genetically engineered His_6-tag, and at the C-termini by vicinal-cysteine handles, and mechanically stretched using a multimode atomic force microscope driven by a Nanoscope IIIa controller and J scanner (Veeco, Santa Barbara, CA). The extended tail domain coated cantilever (Bio-lever; Olympus, Tokyo, Japan) was brought gently near the Ni-NTA-coated (27) glass slide. After successful contact was made with the surface, the cantilever was pulled away at a constant rate (1000 nm/s), typically to 80–100 nm (in the partial-stretch case) and 160–200 nm (in the full-stretch case).

Circular dichroism spectroscopy

Circular dichroism (CD) spectra were recorded on a JASCO J720 spectropolarimeter equipped with a temperature controller using a 0.5 mm cuvette and wavelength range between 190 and 260 nm. All measurements were performed in 20 mM phosphate buffer (pH 7.2) containing 200 mM KCl. For 2,2,2-trifluoroethanol (TFE) titration experiments, the TFE was diluted in 20 mM phosphate buffer (pH 7.2) containing 200 mM KCl. For thermal denaturation experiments, the CD spectra were recorded after the protein samples were incubated for 10 min at different temperature points. Curves were analyzed for a two-state transition between the folded dimer (D) and unfolded fraction (U) (28). Data analyses were performed with Origin software (OriginLab, Northampton, MA).

Differential scanning calorimetry

Differential scanning calorimetry (DSC) measurements were performed using a VP-DSC calorimeter from MicroCal (Northampton, MA). The VP-DSC instrument was run without feedback with at least a 60-min equilibration before each scan. Samples at concentrations in the range of 2.5–5 μM were scanned from 15°C to 55°C with rapid cooling between scans. In all cases, thermal unfolding was irreversible. Measurements were repeated two times to determine reproducibility. The excess heat capacity (C_p) was expressed in kcal $\times$ K^{-1} $\times$ mol^{-1}, where 1.000 cal = 4.184 J. Data conversion and analysis were performed with Origin software (OriginLab).

RESULTS

Protein expression and purification

We expressed the extended tail domains of the *Mm* myosin Va and *Dm* myosin V molecules in BL21(DE3)pLysS and were able to obtain >95% pure protein preparations (see Fig. S1 *A* in the Supporting Material). The protein samples were of high purity and devoid of degradation products, and did not greatly aggregate with time in solution. The samples were loaded on a gel filtration column and appeared as sharp, single peaks (Fig. S1 *C*). The proper dimer formation and refolding of the coiled-coil structure of the segments was confirmed using native gel electrophoresis (Fig. S1 *B*) CD spectra of the segments.

CD measurements

To compare the stabilities of the regions, we performed temperature-dependent CD measurements on the extended tail domains of the myosin V molecules. The effect of temperature on the secondary structure of the extended tail domain of *Mm* myosin Va and *Dm* myosin V was monitored by CD spectroscopy (Figs. 2 and 3). The spectra of extended tail domains shown in Fig. 2 are typical of an α-helical coiled-coil protein, with a double minima at 208 and 222 nm and a ratio of $Ø_{222}/Ø_{208}$ close to 1 (29).

The stability of the extended tail domains was investigated by thermal denaturation, and the ellipticity change was monitored at 222 nm (Fig. 3 *A*). During the increase in temperature, the $Ø_{222}/Ø_{208}$ ratio decreased, which is consistent with a two-state coiled-coil dimer/random coil monomer transition upon heating. Both segments became denatured at relatively low temperatures (T_m = 46°C/31°K for the *Mm*

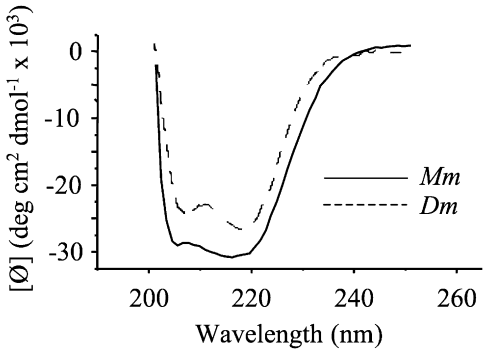

FIGURE 2 CD spectra of *Mm* (*continuous line*) and *Dm* (*dashed line*) extended tail domains.

myosin Va extended tail domain, and 34°C/307°K for the extended tail domain from *Dm* myosin V). The difference between the observed melting temperature of *Mm* myosin Va and *Dm* myosin V extended tail domains was 12°C (Fig. 3 *A*). Thermal unfolding of the extended tail domains was irreversible (Fig. 3, *B* and *C*), which is unexpected for coiled-coil dimers. The normalized $[Ø]_{222}$ value in both cases shows a sigmoidal decrease in the first round of experiments, but the same values are significantly lower in the second, consecutive heat cycle (Fig. 3, *B* and *C*, *solid triangles*), indicating that the unfolding was irreversible during the timescale of the experiment.

We studied the effect of varying the concentration of the extended tail domains on the $Ø_{222}/Ø_{208}$ ratio to evaluate

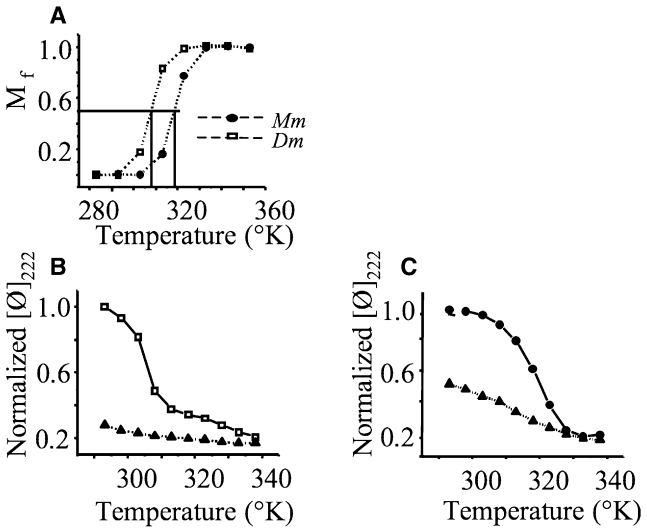

FIGURE 3 Thermal stability and denaturation of extended tail domains. Melting profiles of *Dm* (*open squares*) and *Mm* (*solid circles*) extended tail domains as a function of unfolded fraction (f_U) are shown. (*A*) The T_m values were 46°C/319°K for the *Mm* myosin Va extended tail domain, and 34°C/307°K for the extended tail domain of *Dm* myosin V. (*B* and *C*) The thermal unfolding of extended tail domains is irreversible. The normalized $[Ø]_{222}$ value shows a sigmoidal decrease during the first heat cycle (*B*, *open rectangles*: *Dm* extended tail domain; *C*, *solid circles*: *Mm* extended tail domain. (*B* and *C*, *triangles*) The profile of the second heat cycle indicates that the unfolding was irreversible.

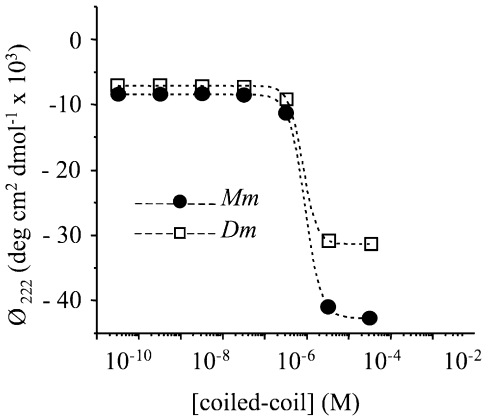

FIGURE 4 Concentration dependence of molar ellipticities at 222 nm. Molar ellipticities at 222 nm of the extended tail domains at various concentrations were measured at 25°C. Open squares and solid circles depict the molar ellipticities of the *Dm* and *Mm* extended tail domains, respectively. The K_d values are 1.38 μM for the *Dm* extended tail domain and 1.61 μM for the *Mm* extended tail domain.

whether coiled-coil formation occurs as a result of increasing concentrations of protein. As shown in Fig. 4, each extended tail domain exhibited a remarkable concentration dependence of the molar ellipticities at 222 nm. We estimated the dissociation constants (K_d) for the *Dm* and *Mm* extended tail domains to be 1.38 and 1.61 μM, respectively, in buffer containing 200 mM KCl. Acetate buffer is known to stabilize coiled-coil structures (30,31). We performed concentration-dependent CD measurements in the presence of 0.6 M sodium acetate to ascertain the effect of acetate buffer on the stability of extended tail domains. The apparent dissociation constants were lower, as expected, but only by ~2-fold (0.79 μM for the *Mm* extended tail domain, and 0.51 μM for the *Dm* extended tail domain; data not shown).

It should be noted that the molar ellipticities in the low-concentration range were $\sim -10{,}000°$ cm^2 dmol^{-1}, not ~ -4000 (the value for a random-coil structure).

To demonstrate the presence of a coiled-coil folding structure in dimers, we performed TFE titration experiments (Fig. 5). TFE is known to stabilize secondary structures, but it disrupts higher-order structures such as coiled coils (32,33). The $[Ø]_{222}/[Ø]_{208}$ ratio was found to change in a sigmoidal manner from ~1.04 in phosphate buffer, pH 3, to ~0.96 in the presence of 80% TFE, indicating a cooperative transition from a two-stranded α-helical coiled coil to a single-stranded α-helix (Fig. 5).

DSC measurements

Thermal unfolding of extended tail domains followed by CD spectroscopy provided information about the thermal stability of the coiled-coil helices within these segments. To further elucidate the structure of the segments, we performed DSC measurements on the extended tail domains.

The unfolding of the extended tail domains of myosin V molecules was irreversible (Fig. 6) and thus could not be

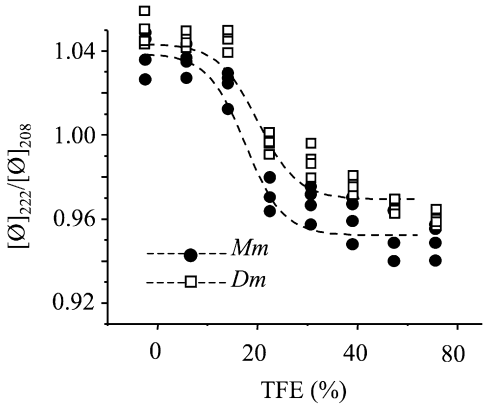

FIGURE 5 Conformational state of the *Dm* and *Mm* extended tail domains. The ellipticity ratio $[Ø]_{222}/[Ø]_{208}$ of ~1.04 in 50 mM phosphate buffer at pH 3, 25°C, indicates a coiled-coil formation, which is disrupted by increasing amounts of TFE, as shown by the sigmoidal decrease of $[Ø]_{222}/[Ø]_{208}$ to ~0.96. Open squares: *Dm* extended tail domain; solid circles: *Mm* extended tail domain. Data points shown are the averages ± SE of four measurements.

analyzed with a two-state (folded-unfolded) model. The T_m values were 46.1°C for the *Mm* myosin Va extended tail domain and 40.6°C for the *Dm* extended tail domain. In similarity to the results of the temperature-dependent CD measurements, the *Mm* extended tail domain is thermally more stable than the *Dm* extended tail domain. The main differences in these curves are the slope and the profile of the initial phase of the curves. The main peaks most likely correspond to the transition of proteins from a native dimer to its denatured conformation, accompanied by the rupture of inter- and intramolecular bonds inside the coiled-coil helix. The peak of the *Mm* myosin Va extended tail domain appears to be sharper and clearer than the peak of thermal denaturation of the *Dm* myosin V extended tail domain. In the case of the *Dm* myosin V extended tail domain, the slope is steeper, which suggests that compared to the processive *Mm* myosin Va extended tail domain, the nonprocessive

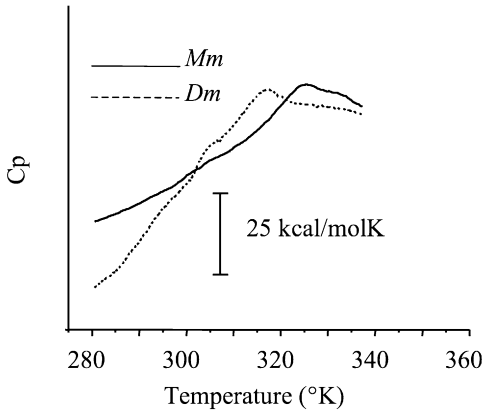

FIGURE 6 DSC curves of the *Mm* myosin Va extended tail domain (*solid line*) and *Dm* myosin V extended tail domain (*dotted line*). The T_m values were 46.1°C (*Mm*) and 40.6°C (*Dm*).

Dm myosin V extended tail domain is more ordered. Thus, although it is likely that both extended tail domains consist of coiled-coil helices and other secondary structures that destabilize before the main unfolding event, the contribution of the noncoiled-coil structure would be greater in the *Dm* myosin V extended tail domain.

Force spectroscopy of coiled-coil segments

The extended tail domains of processive *Mm* myosin Va and nonprocessive *Dm* myosin V were mechanically manipulated with an AFM force probe. The mechanical behaviors of the extended tail domains from processive and nonprocessive molecules were different. In the case of the extended tail domain from the processive *Mm* myosin Va, the force increased very slowly at the beginning of the stretch cycle (Fig. 7 *A*, *upper trace*). The curve shows nonlinear elasticity and usually exhibits an abrupt drop in force, most likely due to unfolding of the coiled-coil structure. After the drop in force, the curve once again shows nonlinear elasticity with a contour length of ~180 nm (Fig. 7 *A*, *upper trace*), which suggests that the full-length extended tail domain has been stretched during the experiment (the calculated contour length

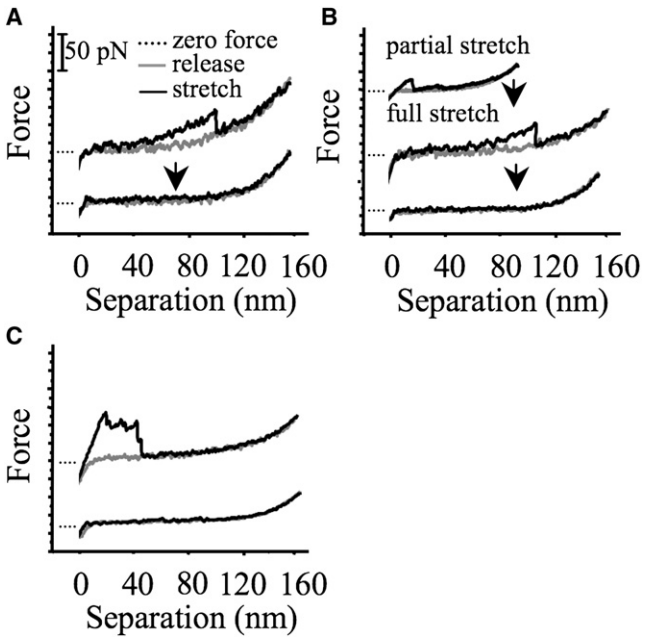

FIGURE 7 Force responses of mechanically manipulated extended tail domains. (*A*) Fully stretched and (*B*) partially and consecutively fully stretched extended tail domains of *Mm* myosin Va molecules. (*A*) After the unfolding event during the full stretch (*upper trace*), the second and consecutive stretches do not show hysteresis (*lower trace*), suggesting that the extended tail domain's unfolding is irreversible. (*B*) The partial stretch (80 nm) shows no sign of hysteresis (*upper trace*) and is highly reproducible. Upon longer stretch (160 nm), the segment unfolds (*middle*), and during consecutive stretches the molecule acts as an unfolded, random polymer chain (*lower trace*). Scale bar: 50 pN. (*C*) Force responses of fully stretched extended tail domains of *Dm* myosin V molecules. In similarity to the *Mm* extended tail domain, after the full stretch (*upper trace*), the second and consecutive stretches do not show hysteresis (*lower trace*).

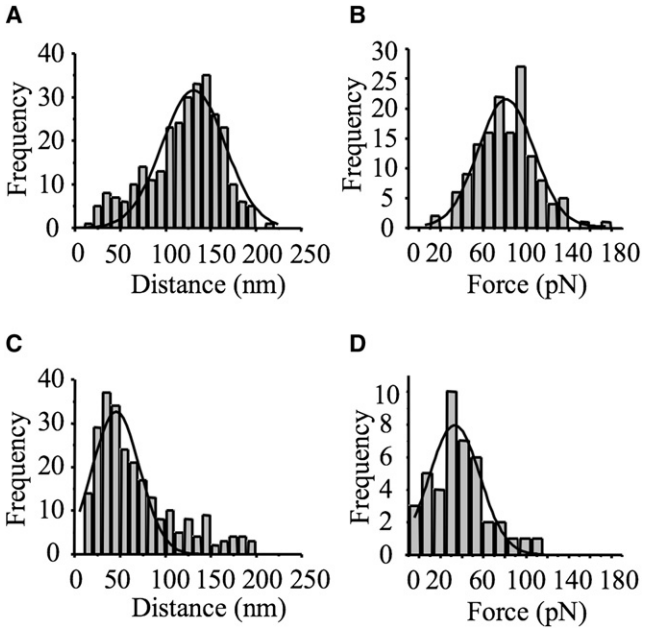

FIGURE 8 Distribution of unfolding events of (*A*) *Mm* and (*C*) *Dm* extended tail domains, and unfolding forces of (*B*) *Mm* and (*D*) *Dm* extended tail domains. Solid lines: Gaussian fits.

of the fully stretched molecule is ~180 nm). The hysteresis of the curve is a result of the irreversible unfolding of the coiled-coil structure. The unfolding force was 82 ± 2.7 pN (mean ± SE, $n = 143$; Fig. 7 *A*, *upper trace*, and Fig. 8 *B*). During the subsequent stretch cycles, the extended tail domain behaved as a random polypeptide chain (Fig. 7 *A*, *lower trace*). The stretch-release curves do not show hysteresis, i.e., under the given experimental conditions, the extended tail domain did not refold to its original structure. The lack of hysteresis during the second and consecutive stretches also proves that the sudden drop in force during the first stretch-release cycle results from the unfolding of a secondary protein structure, and not from peeling the molecule off the surface, since no obvious peeling event is detectable during the second and consecutive stretch-release cycles.

To further investigate the elastic properties of the *Mm* extended tail domain, the pulling distance was reduced (to 80 nm). The partially stretched extended tail domain of *Mm* myosin Va acts as a nonlinear spring (Fig. 7 *B*, *upper trace*). This nonlinear force response is highly reproducible if the molecule is not ''overstretched'' beyond the point of unfolding. During this stretch-release cycle, the force increases very slowly. The curves do not show hysteresis, which suggests that no major domain unfolding occurs during the stretch cycle. If the same molecule is pulled to a longer end-to-end length (Fig. 7 *B*, middle trace), the above-mentioned unfolding event and drop in force occurs. In the consecutive stretch-release cycles that occur after the long extension, the molecule acts as nonlinear spring, as described above (Fig. 7 *B*, *lower trace*).

For the nonprocessive *Dm* myosin V extended tail domain, the force increased immediately after the cantilever tip was detached from the surface (Fig. 7 *C*, *upper trace*). This mechanical response can be characterized as a force plateau with a changing force level during the stretch. The plateau force determined from the difference between the average plateau height and the baseline was 42 ± 3.6 pN (mean ± SE, $n = 42$; Fig. 8 *D* and Fig. 7 *C*, *upper trace*). The hysteresis as observed in the raw data is a result of the unfolding of the coiled-coil and, possibly, other secondary structures within the extended tail domain. As in the case of the *Mm* extended tail domain, the consecutive stretch-release cycles do not show hysteresis (Fig. 7 *C*, *lower trace*).

Histograms were constructed from the distances between the coverslip surface and the point of the abrupt drop in force during the stretch-release cycle (Fig. 8, *A* and *B*). Results were fitted with Gaussian distributions. For the *Mm* myosin Va extended tail domain, the peak of the distribution was 133 ± 2.34 nm (mean ± SE, $n = 291$), whereas in the case of the *Dm* extended tail domain, the peak was at 43 ± 2.87 nm (mean ± SE, $n = 249$).

AFM and electron microscopy imaging

To explore the folded structure of these segments, we performed AFM and electron microscopy (EM) imaging experiments. Fig. 9, *A* and *C*, show the scanned AFM images of the *Mm* myosin Va extended tail domain (Fig. 9 *A*, *lower-right panel*) and the *Dm* myosin V extended tail domain (Fig. 9 *C*, *lower-right panel*). The extended tail domain of the myosin V molecules (Fig. 9, *A* and *C*, *lower-right panel*) appears to be short rods without obvious loops or other folding structures, which is most likely the result of insufficient spatial resolution of the AFM system used for imaging. In comparison, the rotary shadowed EM images of the extended tail domains of *Mm* and *Dm* myosin V molecules (Fig. 9, *A* and *C*, *lower left panel*) look very similar to images recorded with AFM. At the end of the rods on both the scanned AFM and EM images, globular structures very often can be identified. We speculate that the globular structure is a partially unfolded extended tail domain sequence.

The lengths of the extended tail domains were measured from both AFM and negatively stained EM images, and histograms were constructed from the data (Fig. 9, *B* and *D*). For the *Mm* myosin Va extended tail domain, the peak of the distribution was 32.3 ± 0.78 nm (mean ± SE, $n = 54$), whereas in the case of the *Dm* extended tail domain the peak was at 31.7 ± 0.72 nm (mean ± SE, $n = 34$).

EM images of the extended tail domains of *Mm* and *Dm* myosin V molecules were recorded before (Fig. 9, *A* and *C*, *upper-left panel*) and after the samples were heated to 80°C/353°K (Fig. 9, *A* and *C*, *upper-right panel*). The number of extended tail domains was counted in 12 fields of view in each case. In the case of *Mm* extended tail domains, after the heat treatment the number of observed rod-shaped structures on the images decreased by 82%, and instead of rods,

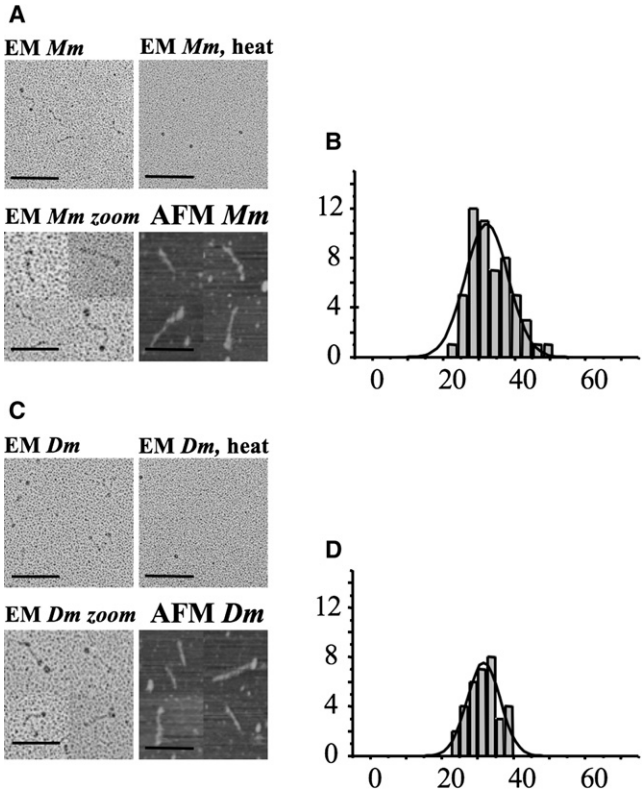

FIGURE 9 AFM and EM images of extended tail domains. (*A*) Upper left: EM image of extended tail domains of *Mm* myosin Va; scale bar: 50 nm. Upper right: EM images of extended tail domains of *Mm* myosin Va after heat treatment; scale bar: 50 nm. Lower left: Negatively-stained EM images of various extended tail domains of *Mm* myosin Va; scale bar: 100 nm. Lower right: AFM images of various extended tail domains of *Mm* myosin Va; scale bar: 100 nm. (*B*) Length distribution of *Mm* myosin Va extended tail domains. (*C*) Upper left: EM image of extended tail domains of *Dm* myosin V; scale bar: 50 nm. Upper right: EM images of extended tail domains of *Dm* myosin V after heat treatment; scale bar: 50 nm. Lower left: EM images of various extended tail domains of *Dm* myosin V; scale bar: 100 nm. Lower right: AFM images of various extended tail domains of *Dm* myosin V; scale bar: 100 nm. (*D*) Length distribution of *Dm* myosin V extended tail domains. Solid lines: Gaussian fits.

globular objects were visible (Fig. 9 *A*, *upper-right panel*). After the heat treatment, the rod-shaped structures completely disappeared in the case of *Dm* extended tail domains. Just as in the former case, globular objects were visible on the EM images (Fig. 9 *C*, *upper-right panel*).

DISCUSSION

The coiled-coil folding motif is a rigid and mechanically stable structure. However, the mechanical properties of coiled-coil structures—especially those present in myosin molecules—are not well characterized. Schwaiger and colleagues (31) stretched a full-length skeletal myosin II with an atomic force microscope and found that the myosin II coiled-coil is an elastic structure that shows little or no hysteresis during the stretch-and-release cycles. Root and colleagues (34) showed that the coiled-coil myosin rod is a truly elastic structure and can be unfolded at forces of ~40 pN.

Mm myosin Va must move its large cargo through a viscous cytoplasm that contains a tangled meshwork of cytoskeletal filaments and membranes, which may prevent instantaneous forward motion of the cargo. If the mechanical properties of the extended tail domain of myosin V (i.e., the tether between the cargo and the motor) were exactly the same as those of the rod of skeletal myosins, the coiled coil would not unfold, the backward force exerted on the motor during the above-mentioned range of motion would equal the stall force, and the myosin V-cargo system would be immobile.

The motion of the cargo-myosin complex is load-dependent, and the load exerted on the motor depends on the elasticity of the tether between the cargo and the motor. Kolomeisky and Fisher (35) applied a two-state model to describe the effects of cargo size and tether elasticity on the stepping characteristics of myosin V. The authors predicted that whereas ATP binding is load-independent, the ADP release and therefore the whole stepping mechanism is dependent on the load applied on the motor. In modeling studies, Schilstra and Martin (36) proposed that a tethered load imposes a gait on the motion of myosin V. These authors used a mathematical model to describe the motion of a cargo-motor system in a viscous environment. In their model, the behavior of this region most likely shows nonlinear elasticity and could be better described with the wormlike chain model (31,37). The authors hypothesized that if the spring element between the cargo and the motor could be considered a nonlinear spring (i.e., soft at the beginning of the stretch cycle and stiff when stretched further), the motion of the myosin Va-vesicle complex in the viscous environment of the cytosol would be highly regular (36).

The most important spring element in the myosin Va-cargo system is likely to be the extended tail domain of the processive myosin molecule. This region consists of predicted (by the PairCoil algorithm) coiled-coil sequences with a few large interruptions (Fig. S1 *D*, *a* and *b*). The coiled-coil content of the intermediate regions is relatively low (277 amino acids at probability values of 0.8 for *Mm* myosin Va, and 148 amino acids at probability values of 0.8 for *Dm* myosin V (Fig. S1 *D*). The calculated lengths of the segments using a value of 0.8 as the threshold for the coiled-coil content, and not considering the intervening sequences, are 41 nm for *Mm* myosin Va and 22 nm for *Dm* myosin V, but the actual length of the segment will also depend on the extension of the loops.

The exact structure of the loop sequences is poorly understood. Secondary structure prediction programs give low values for both α-helix and β-sheet structures, and no consistently obvious domains or other folding units can be identified on AFM or EM images, most likely because of insufficient spatial resolution of the applied techniques. Thus, the extended tail domains of myosin V molecules from mouse and *Drosophila* are very heterogeneous, and they can

be described as a series of springs with different mechanical characteristics linked together.

In this study, we investigated the mechanical behavior of the extended tail domains of processive *Mm* myosin Va and nonprocessive *Dm* myosin V molecules. These molecules exhibit different mechanical behaviors. The processive *Mm* myosin Va is a single-molecule motor that pulls a vesicle through the cytosol in a one-on-one fashion (19), whereas *Dm* myosin V is most likely an ensemble motor, i.e., multiple myosin molecules work as an ensemble to move the same vesicle (26). The single-molecule AFM experiments show that in the case of the extended tail domain of *Mm* myosin Va molecules, at the beginning of the pulling regime, the force increases very slowly. The initial slow rise in force is likely a result of the gradual, low-force unfolding of loose loops between coiled-coil structures. After the ''loose'' structures become completely stretched, the relatively stiff coiled-coil structures begin to strain, and at a given force they unfold (Fig. 7, *A* and *B*). The unfolding event occurs only after the segment has increased 3–4 times in length and at forces much higher than a maximal force exerted with a single myosin Va molecule (Fig. 7, *A* and *B*). Such a spring element completely fulfills the criteria previously described by Schilstra and Martin (36) in their model of processive motion for a myosin V-cargo complex in a viscous environment. It should be noted that the extended tail domains of both of these myosin V molecules exhibit strikingly different mechanical properties compared to those described above for the coiled-coil region of myosin II.

The *Mm* myosin Va extended tail domain is more stable at room temperature than the *Dm* myosin V extended tail domain, as determined by CD measurements. Considering that the mouse is a mammal with a higher core temperature relative to the fruit fly, this finding is not surprising, but it does show that at the beginning of the stretch cycles, the coiled-coil structure of the *Mm* myosin Va molecules most likely remains intact, and the differences between the *Mm* and *Dm* myosin V stretch curves can be explained by the different elastic properties of the other secondary structures present in the extended tail domain.

To explore the detailed structure of both myosin V segments, we performed DSC measurements. The steeper slope of the thermal unfolding curve of the *Dm* myosin V extended tail domain compared to the *Mm* myosin Va coiled-coil segment suggests that the structure of the former is more complex. This finding fits well with the results of the pulling experiments. In the case of the *Mm* myosin Va extended tail domain, the noncoiled-coil structures unfold easily, without any detectable trace on the force-versus-separation or DSC curves. The unfolding of the noncoiled-coil structures in the *Dm* myosin V segment requires more energy, which is detectable in the form of hysteresis and a large plateau on the force-versus-separation traces and the steep initial phase of the DSC curves.

The heat- (38) or force-induced (31) denaturation of coiled-coil segments of the myosin II molecules is known to be a reversible process. In our CD and DSC experiments, the unfolding processes of the extended tail domains of *Mm* myosin Va and *Dm* myosin V molecules were irreversible during the applied timescale. Similarly, in single-molecule force spectroscopy measurements, after the unfolding of the extended tail domains the consecutive stretch curves showed no hysteresis or any other sign of unfolding or refolding events. We speculate that the reason for this phenomenon lies in the sequence and/or unique structure of these myosin rods. The formation of the coiled coil is a highly cooperative process that depends on the sequence of the molecule. Examples of reversible and irreversible unfolding upon heating of coiled-coil domains in kinesin have been reported (39), but such phenomena have also been observed in invasion plasmid antigen D (IpaD) (40). In the above-mentioned heat- and force-induced denaturation studies, the coiled-coil segments were not interrupted by loops or any other folding elements. It is possible that when the register of the highly ordered coiled-coil structure is disturbed by heat or force, the extended tail domains of *Mm* myosin Va and *Dm* myosin V simply do not have enough time to realign and refold during the experiments. It is worthwhile to mention that the force-induced coiled-coil unfolding likely never occurs in vivo, since the stall force is at least one order of magnitude lower than the unfolding force of the extended tail domain.

The data indicate a relatively weak dissociation constant for dimerization of both extended tail domains. The intracellular concentration of myosin Va in the brain is ~3 μM, although in other tissues the myosin V molecules may be less abundant (41). We determined the dissociation constant using only the extended tail domain of the molecule, not the full-length myosin V, where interactions between the globular tail domains of the molecule might affect the stability. When myosin V is activated, it is bound to a cargo (melanophilin), which might greatly influence the monomer-dimer equilibrium. Similarly, in the inactivated state, the tail domain of the molecule folds back to its head, which also might prevent the dissociation of the dimer (for review, see Sellers and Knight (42)).

In addition, our experiments were carried out under ionic conditions commonly employed for in vitro experiments. These conditions do not truly reflect intracellular ionic conditions. For example, cells do not contain significant chloride ions, which are known to be deleterious for coiled-coil stability. However, our measurements allow us to compare the stability of these coiled coils with that of other molecules measured under in vitro conditions. Similar or even weaker dissociation constants have been measured using coiled-coil fragments of motor molecules in kinesin (coiled-coil segments from the stalk domain of *ncd*) (39) or skeletal muscle (43). In conclusion, we think that the low apparent dissociation constant of the segments does not describe the behavior of the full molecule.

We have shown that the extended tail domains of processive *Mm* myosin Va and nonprocessive *Dm* myosin V exhibit different mechanical behaviors. Our results suggest that the

elastic properties of the extended tail domain of single-molecule processive myosin V motors may be crucial for the initiation and support of processive cargo movement in cells. The optimal run length and velocity of the cargo-motor complex moving through a tangled and viscous cytoplasm may be tuned by changing the elastic characteristics of this tether.

As single-molecule vesicle transporters, kinesins and myosins share common features. They have a dimeric structure and walk in a hand-over-hand fashion, which requires that one of the heads must always be attached to the actin or microtubule track to ensure processivity. The stall forces of these single-molecule motors are different, but all of the values are lower than 10 pN (~2–3 pN for myosin V (20,23,25), ~8 pN for kinesins (44,45), and ~5 pN for dyneins (46)). Considering that the cargo sizes and the values of the maximal exerted forces are within the same range, it is not surprising that the presence of elastic elements has been shown in myosin VI (47,48) and kinesin (49) molecules.

Based on our results and those of other researchers, we propose that the presence of an elastic spring element in processive single-molecule vesicle transporters is a common feature of these motors. Future in vitro and in vivo experiments will be required to elucidate the effect of compliant tethers on the mechanics and kinetics of cargo transporters.

SUPPORTING MATERIAL

More materials and methods and a figure are available at http://www.biophysj.org/biophysj/supplemental/S0006-3495(09)01516-1.

We thank Dr. Earl Homsher, Dr. Nico Tjandra, Dr. John A. Hammer 3rd, Dr. Peter Knight, Dr. Ann Ginsburg, Dr. Marie-Paule Strub, Dr. Jeff Forbes, and Dr. Yasuharu Takagi for technical help and valuable comments on the manuscript, and Myoung-Soon Hong for EM images.

REFERENCES

1. Reck-Peterson, S. L., D. W. Provance, Jr., M. S. Mooseker, and J. A. Mercer. 2000. Class V myosins. *Biochim. Biophys. Acta*. 1496:36–51.
2. Vale, R. D. 2003. Myosin V motor proteins: marching stepwise towards a mechanism. *J. Cell Biol.* 163:445–450.
3. Titus, M. A. 1997. Motor proteins: myosin V–the multi-purpose transport motor. *Curr. Biol.* 7:R301–R304.
4. Sellers, J. R. 1999. Myosins. *In* Myosins. J. R. Sellers, editor. Oxford University Press, Oxford, UK. 23–27.
5. Evans, L. L., A. J. Lee, P. C. Bridgman, and M. S. Mooseker. 1998. Vesicle-associated brain myosin-V can be activated to catalyze actin-based transport. *J. Cell Sci.* 111:2055–2066.
6. Tabb, J. S., B. J. Molyneaux, D. L. Cohen, S. A. Kuznetsov, and G. M. Langford. 1998. Transport of ER vesicles on actin filaments in neurons by myosin V. *J. Cell Sci.* 111:3221–3234.
7. Cheney, R. E., M. K. O'Shea, J. E. Heuser, M. V. Coelho, J. S. Wolenski, et al. 1993. Brain myosin-V is a two-headed unconventional myosin with motor activity. *Cell*. 75:13–23.
8. Mehta, A. D., R. S. Rock, M. Rief, J. A. Spudich, M. S. Mooseker, et al. 1999. Myosin-V is a processive actin-based motor. *Nature*. 400:590–593.
9. Veigel, C., F. Wang, M. L. Bartoo, J. R. Sellers, and J. E. Molloy. 2002. The gated gait of the processive molecular motor, myosin V. *Nat. Cell Biol.* 4:59–65.
10. Krementsov, D. N., E. B. Krementsova, and K. M. Trybus. 2004. Myosin V: regulation by calcium, calmodulin, and the tail domain. *J. Cell Biol.* 164:877–886.
11. Lu, H., E. B. Krementsova, and K. M. Trybus. 2006. Regulation of myosin V processivity by calcium at the single molecule level. *J. Biol. Chem.* 281:31987–31994.
12. Wang, F., K. Thirumurugan, W. F. Stafford, J. A. Hammer, 3rd, P. J. Knight, et al. 2004. Regulated conformation of myosin V. *J. Biol. Chem.* 279:2333–2336.
13. Thirumurugan, K., T. Sakamoto, J. A. Hammer, 3rd, J. R. Sellers, and P. J. Knight. 2006. The cargo-binding domain regulates structure and activity of myosin 5. *Nature*. 442:212–215.
14. Wu, X. S., K. Rao, H. Zhang, F. Wang, J. R. Sellers, et al. 2002. Identification of an organelle receptor for myosin-Va. *Nat. Cell Biol.* 4:271–278.
15. Li, X. D., H. S. Jung, Q. Wang, R. Ikebe, R. Craig, et al. 2008. The globular tail domain puts on the brake to stop the ATPase cycle of myosin Va. *Proc. Natl. Acad. Sci. USA*. 105:1140–1145.
16. Liu, J., D. W. Taylor, E. B. Krementsova, K. M. Trybus, and K. A. Taylor. 2006. Three-dimensional structure of the myosin V inhibited state by cryoelectron tomography. *Nature*. 442:208–211.
17. De La Cruz, E. M., A. L. Wells, S. S. Rosenfeld, E. M. Ostap, and H. L. Sweeney. 1999. The kinetic mechanism of myosin V. *Proc. Natl. Acad. Sci. USA*. 96:13726–13731.
18. Rogers, S. L., R. L. Karcher, J. T. Roland, A. A. Minin, W. Steffen, et al. 1999. Regulation of melanosome movement in the cell cycle by reversible association with myosin V. *J. Cell Biol.* 146:1265–1276.
19. Sellers, J. R., and C. Veigel. 2006. Walking with myosin V. *Curr. Opin. Cell Biol.* 18:68–73.
20. Rief, M., R. S. Rock, A. D. Mehta, M. S. Mooseker, R. E. Cheney, et al. 2000. Myosin-V stepping kinetics: a molecular model for processivity. *Proc. Natl. Acad. Sci. USA*. 97:9482–9486.
21. Rosenfeld, S. S., and H. L. Sweeney. 2004. A model of myosin V processivity. *J. Biol. Chem.* 279:40100–40111.
22. Veigel, C., S. Schmitz, F. Wang, and J. R. Sellers. 2005. Load-dependent kinetics of myosin-V can explain its high processivity. *Nat. Cell Biol.* 7:861–869.
23. Purcell, T. J., H. L. Sweeney, and J. A. Spudich. 2005. A force-dependent state controls the coordination of processive myosin V. *Proc. Natl. Acad. Sci. USA*. 102:13873–13878.
24. Bausch, A. R., W. Moller, and E. Sackmann. 1999. Measurement of local viscoelasticity and forces in living cells by magnetic tweezers. *Biophys. J.* 76:573–579.
25. Clemen, A. E., M. Vilfan, J. Jaud, J. Zhang, M. Barmann, et al. 2005. Force-dependent stepping kinetics of myosin-V. *Biophys. J.* 88:4402–4410.
26. Toth, J., M. Kovacs, F. Wang, L. Nyitray, and J. R. Sellers. 2005. Myosin V from *Drosophila* reveals diversity of motor mechanisms within the myosin V family. *J. Biol. Chem.* 280:30594–30603.
27. Yasuda, R., H. Noji, K. Kinosita, Jr., and M. Yoshida. 1998. F1-ATPase is a highly efficient molecular motor that rotates with discrete 120° steps. *Cell*. 93:1117–1124.
28. Hodi, Z., A. L. Nemeth, L. Radnai, C. Hetenyi, K. Schlett, et al. 2006. Alternatively spliced exon B of myosin Va is essential for binding the tail-associated light chain shared by dynein. *Biochemistry*. 45: 12582–12595.
29. Lau, S. Y., A. K. Taneja, and R. S. Hodges. 1984. Synthesis of a model protein of defined secondary and quaternary structure. Effect of chain length on the stabilization and formation of two-stranded α-helical coiled-coils. *J. Biol. Chem.* 259:13253–13261.
30. Stafford, 3rd, W. F. 1985. Effect of various anions on the stability of the coiled coil of skeletal muscle myosin. *Biochemistry*. 24:3314–3321.
31. Schwaiger, I., C. Sattler, D. R. Hostetter, and M. Rief. 2002. The myosin coiled-coil is a truly elastic protein structure. *Nat. Mater.* 1:232–235.
32. Sonnichsen, F. D., J. E. Van Eyk, R. S. Hodges, and B. D. Sykes. 1992. Effect of trifluoroethanol on protein secondary structure: an NMR

and CD study using a synthetic actin peptide. *Biochemistry*. 31:8790–8798.

33. Bodkin, M. J., and J. M. Goodfellow. 1996. Hydrophobic solvation in aqueous trifluoroethanol solution. *Biopolymers*. 39:43–50.
34. Root, D. D., V. K. Yadavalli, J. G. Forbes, and K. Wang. 2006. Coiled-coil nanomechanics and uncoiling and unfolding of the superhelix and α-helices of myosin. *Biophys. J*. 90:2852–2866.
35. Kolomeisky, A. B., and M. E. Fisher. 2003. A simple kinetic model describes the processivity of myosin-v. *Biophys. J*. 84:1642–1650.
36. Schilstra, M. J., and S. R. Martin. 2006. An elastically tethered viscous load imposes a regular gait on the motion of myosin-V. Simulation of the effect of transient force relaxation on a stochastic process. *J. R. Soc. Interface*. 3:153–165.
37. Bustamante, C., J. F. Marko, E. D. Siggia, and S. Smith. 1994. Entropic elasticity of λ-phage DNA. *Science*. 265:1599–1600.
38. Zolkiewski, M., M. J. Redowicz, E. D. Korn, J. A. Hammer, 3rd, and A. Ginsburg. 1997. Two-state thermal unfolding of a long dimeric coiled-coil: the *Acanthamoeba* myosin II rod. *Biochemistry*. 36: 7876–7883.
39. Makino, T., H. Morii, T. Shimizu, F. Arisaka, Y. Kato, et al. 2007. Reversible and irreversible coiled coils in the stalk domain of ncd motor protein. *Biochemistry*. 46:9523–9532.
40. Espina, M., S. F. Ausar, C. R. Middaugh, W. D. Picking, and W. L. Picking. 2006. Spectroscopic and calorimetric analyses of invasion plasmid antigen D (IpaD) from *Shigella flexneri* reveal the presence of two structural domains. *Biochemistry*. 45:9219–9227.
41. Geething, N. C., and J. A. Spudich. 2007. Identification of a minimal myosin Va binding site within an intrinsically unstructured domain of melanophilin. *J. Biol. Chem*. 282:21518–21528.
42. Sellers, J. R., and P. J. Knight. 2007. Folding and regulation in myosins II and V. *J. Muscle Res. Cell Motil*. 28:363–370.
43. Malnasi-Csizmadia, A., E. Shimony, G. Hegyi, A. G. Szent-Gyorgyi, and L. Nyitray. 1998. Dimerization of the head-rod junction of scallop myosin. *Biochem. Biophys. Res. Commun*. 252:595–601.
44. Svoboda, K., C. F. Schmidt, B. J. Schnapp, and S. M. Block. 1993. Direct observation of kinesin stepping by optical trapping interferometry. *Nature*. 365:721–727.
45. Svoboda, K., and S. M. Block. 1994. Force and velocity measured for single kinesin molecules. *Cell*. 77:773–784.
46. Schmitz, K. A., D. L. Holcomb-Wygle, D. J. Oberski, and C. B. Lindemann. 2000. Measurement of the force produced by an intact bull sperm flagellum in isometric arrest and estimation of the dynein stall force. *Biophys. J*. 79:468–478.
47. Spink, B. J., S. Sivaramakrishnan, J. Lipfert, S. Doniach, and J. A. Spudich. 2008. Long single α-helical tail domains bridge the gap between structure and function of myosin VI. *Nat. Struct. Mol. Biol*. 15:591–597.
48. Rock, R. S., B. Ramamurthy, A. R. Dunn, S. Beccafico, B. R. Rami, et al. 2005. A flexible domain is essential for the large step size and processivity of myosin VI. *Mol. Cell*. 17:603–609.
49. Jaud, J., F. Bathe, M. Schliwa, M. Rief, and G. Woehlke. 2006. Flexibility of the neck domain enhances kinesin-1 motility under load. *Biophys. J*. 91:1407–1412.